Array Configuration Effect on the Spatial Correlation of MU-MIMO Channels in NLoS Environments

N.B. When citing this work, cite the original published paper.

(article starts on next page)

Array Configuration Effect on the Spatial Correlation of MU-MIMO Channels in NLoS Environments

N. Amani[*†], A. Farsaei[†], U. Gustavsson[‡], T. Eriksson[*] F. M. J. Willems[†], M. V. Ivashina[*], R. Maaskant[*†]
[*]Department of Electrical Engineering, Chalmers University of Technology, Gothenburg, Sweden, anavid@chalmers.se
[†]Department of Electrical Engineering, Eindhoven University of Technology (TU/e), Eindhoven, The Netherlands
[‡]Ericsson Research, Gothenburg, Sweden

Abstract—**In this paper, three different base-station antenna (BSA) configurations are compared in terms of inter-user spatial correlation in a two dimensional (2D) non-line-of-sight (NLoS) environment. The three configurations are: (i) a regular uniform linear array (ULA); (ii) a periodic sparse array; and (iii) an aperiodic sparse array. Electromagnetic modeling of the NLoS channel is proposed where scatterers are considered as resonant dipoles confined in clusters of scatterers (CoSs). While the probability of facing highly correlated user-equipments (UEs) in a multi-user multiple-input multiple-output (MU-MIMO) system is decreasing as the richness of mutipath increases, the sparsity (increased inter-element spacing) is seen to be capable of reducing this probability as well. This is due to the larger spatial variations experienced by the sparse array. Moreover, the results show that further improvement can be achieved by deploying an aperiodic distribution of antenna elements into the sparse antenna aperture.**

Index Terms—**Multi-user multiple-input multiple-output (MU-MIMO), non-line-of-sight (NLoS), sparse array, spatial correlation.**

Fig. 1. NLoS multi-user MIMO channel where black dots, representing scatterers, are modeled as resonant dipoles.

I. INTRODUCTION

Line-of-sight (LoS) communication is more reliable at mm-wave frequencies due to the higher diffraction and penetration losses and also a larger path-loss in a non-line-of-sight (NLoS) environment. However, a LoS propagation environment is not guaranteed by nature. Based on the channel models recognized in the scientific literature, the LoS probability decreases as the link distance increases in both urban micro- and macro-cells (UMi, UMa) [1]. An independent and identically distributed (i.i.d.) Rayleigh fading channel, based on the Clarke's model [2], is the most commonly considered channel model is the literature. In [3] it is shown that, under this assumption a multi-user multiple-input multiple-output (MU-MIMO) system employing unlimited number of antennas at the base station theoretically offers interference-free communication, known as favourable propagation, while a conjugate-transpose precoding/combining is deployed. This mutual orthogonality among channel vectors of user equipments (UEs) occurs due to the assumption of i.i.d. fading channels and the law of large numbers. However, in practice the number of base station antennas is limited and the propagation environment is not necessarily favourable [4], [5].
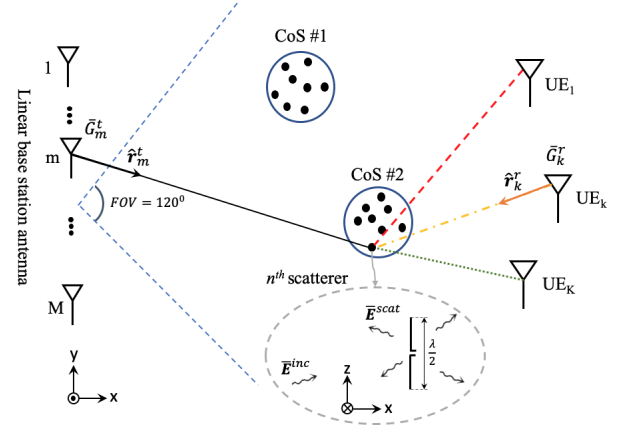
Spatial correlation among UEs has been observed as a degrading factor, which reduces the downlink sum-rate and increases the dynamic range of the power distribution across the array while linear precoders are applied [6]–[8]. Although in a LoS propagation the correlation depends on the angular-separation between UEs, the richness of scattering is a more critical parameter for the system sum-rate in a NLoS scenario [6]. Deploying more antennas at the base station for an improved spatial resolution is a costly solution since it requires more hardware. Nonetheless, given the number of antennas, a larger inter-element spacing (d) can be used as an alternative [9], [10].

In this paper, the effect of sparsity and aperiodicity at the base station antenna (BSA), with a fixed number of elements, on the correlation among two UEs is investigated in a NLoS scenario. Scatterers in the NLoS environment are modeled as half-wavelength dipoles confined in randomly localized clusters of scatterers (CoSs). For a fixed number of dipole scatterers, the richness of multipath in a NLoS environment is adjustable by changing the number of CoSs and hence their density. An analytical transfer function is proposed to compute the scattered field from the dipole scatterers. This physical model enables us to calculate the resultant received

open-circuit voltage at the UEs through all the scatterers. The validity of the transfer function is confirmed through a full-wave simulation.

Employing the proposed electromagnetic (EM) model, three array configurations are examined in NLoS environments with different richness of multipath, which are realized by different number of CoSs. This investigation is carried out by computing the cumulative distribution function (CDF) of the spatial correlation between two UEs in a Monte Carlo simulation. In comparison with a conventional uniform linear array (ULA) with a half-wavelength spacing, an increased inter-element spacing ($d > 0.5\lambda$, where λ is a wavelength) improves the CDF curves of the correlation, specifically, in poor multipath environments. Meanwhile, a non-uniform sparse array is seen to improve the CDF curves further. It is observed that, as the richness of multipath increases the improvement of the CDF curves by the sparse arrays reduces.

II. NLoS Channel Model and Spatial Correlation

A simplified generic EM model to emulate a multipath environment is proposed here. A MU-MIMO system in a NLoS environment is comprised of M elements at the BSA ($m = 1, \ldots, M$), N scatterers ($n = 1, \ldots, N$) and K UEs ($k = 1, \ldots, K$). Multipath components often arrive in clusters based on the mm-wave channel modeling [11]. Therefore, we consider randomly distributed CoSs inside the field-of-view (FoV). Each single-bounce scatterer is modeled by a resonant 0.5λ dipole [12]. For simplicity and without loss of generality, we consider a two-dimensional (2D) problem where dipole scatterers are prependicular to the plane of interest. The incident electric field from the BSA ($\bar{E}^{\text{inc}}$) is considered parallel to the dipole, which scatters the field $\bar{E}^{\text{scat}}$ omni-directionally in the H-plane of the dipole. We further assume that the scattering pattern is the same as the transmitting pattern. Fig. 1 shows the EM model of a NLoS MU-MIMO channel. The open-circuit voltage at the dipole scatterer due to the $\bar{E}^{\text{inc}}$ is [13]

$$V_{\text{d}}^{\text{oc}} = \frac{-2j\lambda}{\eta} \left[\frac{\bar{G}_n^r(\hat{\mathbf{r}}_n^r)}{I_{\text{d}}^{\text{t}}} \right] \bar{E}^{\text{inc}}, \tag{1}$$

where η, I_{d}^{t}, and $\bar{G}(\hat{\mathbf{r}})$ are the free space impedance, the dipole excitation current in the transmitting mode[1] and its corresponding far-field function in the direction of incident plane wave, respectively[2]. The far-field function is related to the electric field ($\bar{E}^{\text{scat}}$) by [13, Eq. (2.39)]:

$$\bar{G}(\hat{\mathbf{r}}) = \bar{E}^{\text{scat}} r e^{j\beta r}, \tag{2}$$

where r denotes the distance between the observation point, where the scattered field is being measured, and the dipole scatterer. Afterwards, the short-circuit current due to the induced open-circuit voltage in the receiving mode is considered as the source current for the scattered field from the dipole

[1] $(.)^{\text{t}}$ and $(.)^{\text{r}}$ represent transmit and receive modes, respectively.
[2] Field vectors are denoted by an overbar while other type of vectors are represented by boldface lowercase letters. $\hat{\mathbf{r}}$ is the unit vector in the spherical coordinate system [13].
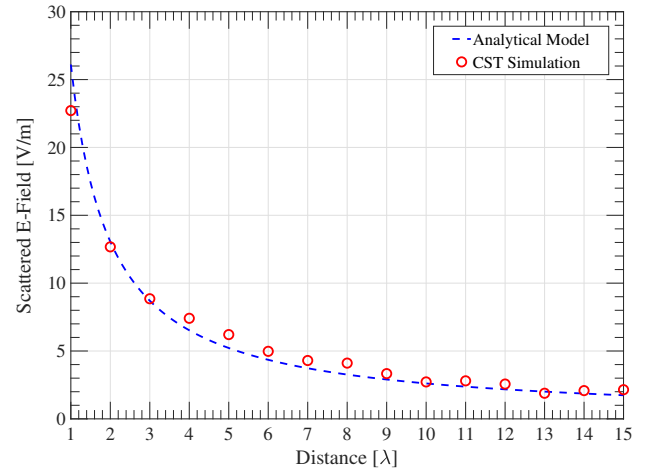

Fig. 2. Scattered E-field from a short circuited resonant dipole (0.5λ thin cylindrical bar) illuminated by a plane wave with $E_z^{\text{inc}} = 100$ V/m. The dipole is z-oriented at the origin of the coordinate system and the scattered field is measured along the y-axis ($E_z^{\text{scat}}|_{x=z=0}$).

scatterer in the transmitting mode, i.e., $I_{\text{d}}^{\text{sc}} = -I_{\text{d}}^{\text{t}}$. Therefore, the accepted power (P_{acc}) at the dipole antenna terminals is

$$P_{\text{acc}} = \frac{|V_{\text{d}}^{\text{oc}}|^2}{2\mathfrak{Re}\{Z_{\text{d}}\}} = \frac{|I_{\text{d}}^{\text{t}}|^2 \mathfrak{Re}\{Z_{\text{d}}\}}{2}, \tag{3}$$

where Z_{d} is the dipole input impedance. By combining (1), (2) and (3)

$$P_{\text{acc}} = \frac{\lambda}{\eta} r \left| \bar{E}^{\text{scat}} \right| \left| \bar{E}^{\text{inc}} \right|. \tag{4}$$

Besides, a half-wavelength resonant dipole has a gain of 2.15 dBi, which is related to the field strength as

$$G = \frac{\frac{1}{2\eta} \left| \bar{E}^{\text{scat}} \right|^2 r^2}{\frac{P_{\text{acc}}}{4\pi}}. \tag{5}$$

So,

$$P_{\text{acc}} = \frac{2\pi r^2 \left| \bar{E}^{\text{scat}} \right|^2}{\eta 10^{(G_{\text{dBi}}/10)}} \approx \frac{r^2 \left| \bar{E}^{\text{scat}} \right|^2}{98.4}. \tag{6}$$

Upon inserting (6) into (4)

$$\left| \bar{E}^{\text{scat}} \right| = \frac{98.4\lambda}{\eta r} \left| \bar{E}^{\text{inc}} \right|, \tag{7}$$

where the field transfer function becomes dependent on distance and frequency, as follows

$$T(\lambda, r) = \frac{98.4\lambda}{\eta r}. \tag{8}$$

Assuming that all scatterers can be modeled as resonant dipoles and since the phase difference between the multipath components contributes to the fading effect, (7) can be rewritten as

$$\bar{E}^{\text{scat}} = T(\lambda, r) \bar{E}^{\text{inc}} e^{-j\beta r}. \tag{9}$$
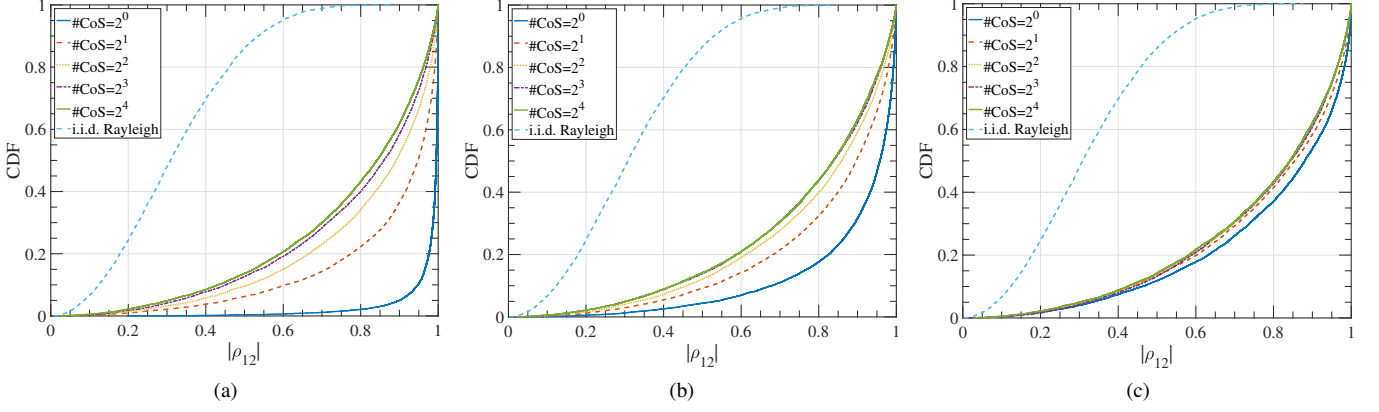
Fig. 3. CDF plots of the spatial correlation among two users through a Monte Carlo simulation in a NLoS environment with different number of CoSs, using an eight-element: (a) conventional ULA with $d = 0.5\lambda$; (b) periodic sparse array with $d = 1.5\lambda$; (c) aperiodic sparse array with the same aperture size as (b).

It should be noted that, $\bar{E}^{\text{inc}}$ is taken at the dipole scatterer and r is the distance away from this scatterer where $\bar{E}^{\text{scat}}$ is observed.

In order to validate (8), a full-wave simulation is conducted in CST Microwave Studio [14]. A very thin z-oriented short-circuited dipole (cylindrical bar) is located at the origin of the coordinate system. The dipole is illuminated by a plane wave with z-polarized electric field $E_z^{\text{inc}} = 100$ V/m. Afterwards, the scattered field along the y-axis ($E_z^{\text{scat}}|_{x=z=0}$) from the dipole is computed at different distances in CST using field probes. The measured values of the scattered field in the full-wave simulation agree well with the analytical curve calculated by (9) in Fig. 2.

Under the narrowband communication assumption, the proposed EM modeling approach can be deployed to emulate the multipath effect in a multi-scatterer NLoS scenario. Considering M elements at the BSA, N scatterers and K single antenna UEs inside the FoV, r_{nm} denotes the distance between the n-th scatterer and the m-th BSA antenna element while r_{kn} represents the distance between the k-th UE and the n-th scatterer. Hence, the NLoS received voltage at the k-th UE due to the m-th antenna element through the n-th scatterer, employing (9), can be represented as

$$
\begin{aligned}
V_{k,n,m}^{\text{oc}} &= \frac{-2j\lambda}{\eta} \left[\frac{\bar{G}_k^r(\hat{\mathbf{r}}_k^r)}{I_k^t} \right] \bar{E}^{\text{scat}} \\
&= \frac{-2j\lambda}{\eta} \left[\frac{\bar{G}_k^r(\hat{\mathbf{r}}_k^r)}{I_k^t} \right] \frac{98.4\lambda}{\eta r_{kn}} \bar{E}_m^{\text{inc}} e^{-j\beta r_{kn}} \\
&= \frac{-196.8j\lambda^2}{\eta^2} \left[\frac{\bar{G}_k^r(\hat{\mathbf{r}}_k^r)\bar{G}_m^t(\hat{\mathbf{r}}_m^t)}{I_k^t} \right] \frac{e^{-j\beta(r_{kn}+r_{nm})}}{(r_{kn}r_{nm})}.
\end{aligned}
\tag{10}
$$

The entries of channel vectors (from the m-antenna to the k-th UE) can be computed using (10) by adding up the received open-circuit voltages through all the scatterers. Hence, $\mathbf{h}_k = [V_{1,1}^{\text{oc}}, V_{1,2}^{\text{oc}}, \ldots, V_{1,M}^{\text{oc}}]^T$, where $(.)^T$ is the transposition operator, can be calculated by

$$
V_{k,m}^{\text{oc}} = \sum_{n=1}^{N} V_{k,n,m}^{\text{oc}}
\tag{11}
$$

which incorporates the small-scale fading effect.

In [7] it is shown that how the sum-rate of a MU-MIMO system is being decreased as the correlation among two users increases, while linear precoders are applied. The normalized spatial correlation between two users can be computed by:

$$
\rho_{12} = \left| \frac{\mathbf{h}_1^H \mathbf{h}_2}{\|\mathbf{h}_1\| \|\mathbf{h}_2\|} \right|,
\tag{12}
$$

where $\mathbf{h}_1$ and $\mathbf{h}_2$ represent the channel vectors of the UE$_1$ and UE$_2$, respectively, and $(.)^H$ is the Hermitian operator. In the following section the ρ_{12} is being studied for different BSA configurations with the proposed EM modeling of the NLoS environment.

III. SIMULATION RESULTS

An eight-element linear BSA array, operating at 28 GHz, is assumed to have a $120°$ sectorial FoV within which the location of CoSs and single-antenna UEs with omni-directional radiation patterns are randomly defined, with a uniform distribution. BSA elements with flat-top radiation patterns inside the FoV are assumed to experience a negligible mutual coupling effect. The coverage area (D) ranges from one to twenty Fraunhofer distances (FD). For the sake of a fair comparison, the number of scatterers remains the same in all simulation scenarios. A total number of $N = 2^4$ scatterers are spread in different number of CoSs, which varies from 2^0 to 2^4, in intervals of powers-of-two (see Fig. 1 for the case of #CoS = 2). One CoS means that all scatterers are gathered in one cluster. It mimics a poor scattering environment with small spatial variations. On the other hand, when the number of scatterers and CoSs are equal, all scatterers are getting complete freedom to be located anywhere in the visible region. This increases the spatial variations and can be interpreted as a rich multipath medium.

In a Monte Carlo simulation, channel vectors are calculated for 100 realizations of both CoSs and the UEs ($K = 2$). Hence, the correlation among the two channel vectors are computed for 10^4 simulation runs. Fig. 3 shows the CDF plots of the correlation, computed for three BSA configurations: (i) conventional ULA with $d = 0.5\lambda$, (ii) periodic sparse array with $d = 1.5\lambda$, and (iii) aperiodic sparse array with the same aperture size of (ii). A random sparse array is utilized in (iii) where the minimum allowable inter-element spacing is 0.5λ. As it is illustrated in Fig. 3, as a general trend the probability of facing highly correlated UEs decreases when the number of CoSs increases. That is due to the larger spatial variations experienced by the BSA [6]. For all three BSAs, the performance in terms of correlation remains the same in an i.i.d. Rayleigh fading channels and almost a negligible improvement is observed in the rich scattering environment (#CoS $= 2^4$). However, the increased inter-element spacing improves the CDF curves of ρ_{12} in a NLoS environment with a small number of CoSs where the spatial variations are not sufficiently large. This can be observed by comparing Figs. 3(a) and (b) when the number of CoSs is limited. In addition, this improvement is more pronounced by the aperiodic sparse array in NLoS environments with small spatial variations, shown in Fig. 3(c).

IV. CONCLUSION

An EM model of a NLoS environment by considering single-bounce scatterers as half-wavelength resonant dipoles has been presented. A transfer function has been derived to calculate the scattered field from the dipole scatterers. Afterwards, the potential advantages of both periodic and aperiodic sparse arrays in a MU-MIMO system have been investigated by means of CDF plots of the correlation among two UEs in NLoS environments with different richness of multipath. It has been shown that the sparsity together with aperiodicity significantly reduces the probability of facing highly correlated UEs in a relatively poor scattering improvement. On the other hand, the advantage of sparse arrays over the conventional ULA with 0.5λ spacing has been minimal in a rich scattering scenario due to the high spatial variations provided by the environment.

REFERENCES

[1] T. S. Rappaport, Y. Xing, G. R. MacCartney, A. F. Molisch, E. Mellios, and J. Zhang, "Overview of millimeter wave communications for fifth-generation (5G) wireless networks—with a focus on propagation models," *IEEE Trans. Antennas Propag.*, vol. 65, no. 12, pp. 6213–6230, Dec. 2017.

[2] R. Clarke, "A statistical theory of mobile-radio reception," *Bell system technical journal*, vol. 47, no. 6, pp. 957–1000, 1968.

[3] T. L. Marzetta, "Noncooperative cellular wireless with unlimited numbers of base station antennas," *IEEE Trans. Wireless Commun.*, vol. 9, no. 11, pp. 3590–3600, Nov. 2010.

[4] X. Gao, O. Edfors, F. Rusek, and F. Tufvesson, "Linear pre-coding performance in measured very-large MIMO channels." in *Proc. IEEE Veh. Tech. Conf.*, Sep. 2011, pp. 1–5.

[5] F. Kaltenberger, D. Gesbert, R. Knopp, and M. Kountouris, "Correlation and capacity of measured multi-user MIMO channels," in *Proc. IEEE 19th Int. Symp. on Personal, Indoor and Mobile Radio Commun. (PIMRC)*, Sep. 2008, pp. 1–5.

[6] X. Gao, O. Edfors, F. Rusek, and F. Tufvesson, "Massive MIMO performance evaluation based on measured propagation data," *IEEE Trans. Wireless Commun.*, vol. 14, no. 7, pp. 3899–3911, Jul. 2015.

[7] A. Farsaei, A. Alvarado, F. Willems, and U. Gustavsson, "An improved dropping algorithm for line-of-sight massive MIMO with max-min power control," *IEEE Commun. Lett.*, vol. 23, no. 6, pp. 1109–1112, Jun. 2019.

[8] N. Amani, A. A. Glazunov, M. V. Ivashina, and R. Maaskant, "Per-antenna power distribution of a zero-forcing beamformed ULA in pure LOS MU-MIMO," *IEEE Commun. Lett.*, vol. 22, no. 12, pp. 2515–2518, Dec. 2018.

[9] G. Dahman, J. Flordelis, and F. Tufvesson, "Experimental evaluation of the effect of BS antenna inter-element spacing on MU-MIMO separation," in *Proc. IEEE Int. Conf. Commun. (ICC)*, Jun. 2015, pp. 1685–1690.

[10] N. Amani, R. Maaskant, and W. Van Cappellen, "On the sparsity and aperiodicity of a base station antenna array in a downlink MU-MIMO scenario," in *Proc. Int. Symp. Antennas Propag. (ISAP)*, Oct. 2018, pp. 1–2.

[11] M. Peter, K. Haneda, S. L. H. Nguyen, A. Karttunen, J. Järveläinen, A. Bamba, R. D' Errico, J. Medbo, U. F, S. Jaeckel, I. N, J. Luo, M. Rybakowski, C. Diakhate, J. Conrat, A. Naehring, S. Wu, A. Goulianos, and E. Mellios, "Measurement results and final mmMAGIC channel models," *Deliverable D2.2*, May. 2017, [online]. Available:https://bscw.5g-mmmagic.eu/pub/bscw.cgi/d202656/mmMAGIC_D2_2.pdf.

[12] M. E. Bialkowski, P. Uthansakul, K. Bialkowski, and S. Durrani, "Investigating the performance of MIMO systems from an electromagnetic perspective," *Microw. Opt. Tech. Lett.*, vol. 48, no. 7, pp. 1233–1238, Jul. 2006.

[13] P.-S. Kildal, *Foundations of Antenna Engineering: A Unified Approach for Line-of-Sight and Multipath*. Artech House, 2015.

[14] Computer Simulation Technology, "CST Microwave Studio 2018," *https://www.cst.com/*, 2018.